International Journal of Modern Physics D

Neutrino induced reactions in core-collapse supernovae: effects on the electron fraction.

M. M. Saez
Facultad de Ciencias Astronómicas y Geofísicas, University of La Plata. Paseo del Bosque S/N 1900, La Plata, Argentina.
msaez@fcaglp.unlp.edu.ar

O. Civitarese
Dept. of Physics, University of La Plata, c.c. 67 1900, La Plata, Argentina
osvaldo.civitarese@fisica.unlp.edu.ar

M. E. Mosquera
Dept. of Physics, University of La Plata, c.c. 67
Facultad de Ciencias Astronómicas y Geofísicas, University of La Plata. Paseo del Bosque S/N 1900, La Plata, Argentina

Received Day Month Year
Revised Day Month Year

Neutrino induced reactions are a basic ingredient in astrophysical processes like star evolution. The existence of neutrino oscillations affects the rate of nuclear electroweak decays which participates in the chain of events that determines the fate of the star. Among the processes of interest, the production of heavy elements in core-collapse supernovae is strongly dependent upon neutrino properties, like the mixing between different species of neutrinos.

In this work we study the effects of neutrino oscillations upon the electron fraction as a function of the neutrino mixing parameters, for two schemes: the $1+1$ scheme (one active neutrino and one sterile neutrino) and the $2+1$ scheme (two active neutrinos and one sterile neutrino). We have performed this analysis considering a core-collapse supernovae and determined the physical conditions needed to activate the nuclear reaction chains involved in the r-process. We found that the interactions of the neutrinos with matter and among themselves and the initial amount of sterile neutrinos in the neutrinosphere might change the electron fraction, therefore affecting the onset of the r-process. We have set constrains on the active-sterile neutrino mixing parameters. They are the square-mass-difference Δm^2_{14}, the mixing angle $\sin^2 2\theta_{14}$, and the hindrance factor ξ_s for the occupation of sterile neutrinos. The calculations have been performed for different values of X_α, which is the fraction of α-particles. For $X_\alpha = 0$ the r-process is taking place if $\Delta m^2_{14} \geq 2\,\mathrm{eV}^2$, $\sin^2 2\theta_{14} < 0.8$ and $\xi_s < 0.5$. For larger values of X_α the region of parameters is strongly reduced. The present results are compared to results available in the literature.

Keywords: Sterile neutrino, supernova, r-process

26.30.-k,26.30.Hj,26.50.+x,26.30.Jk

1. Introduction

Several experiments, like LSND,[1] SK,[2] SNO,[3] and MiniBooNE[4] among others,[5–10] have provided evidences of neutrino oscillations caused by non-zero neutrino masses. In particular, the results of LSND and MiniBooNE are compatible with the inclusion of at least an extra sterile neutrino.[11–13]

The consequences of the inclusion of massive neutrinos and sterile neutrinos in different astrophysical scenarios have been examined recently.[14–16] The presence of massive neutrinos affects the rates of nuclear reactions where they participate, therefore a reformulation of the weak decay rates in terms of neutrino oscillation parameters and couplings is needed to explain several astrophysical processes, such as Big Bang Nucleosynthesis[17] and nuclear reaction chains in stellar media.[18,19] In supernovae, near the stellar-core, the neutrino flux might suffer conversions to the sterile sector causing a reduction in the number of electron neutrinos.[20] The effects of the active-active and active-sterile oscillations in supernova explosions have been studied by several authors.[21–29] It allows to analyse the behaviour of matter at high densities and test properties of neutrino physics.[22,25] The process responsible for the production of nuclei heavier than iron is the rapid neutron-capture process or r-process. To be effective the reaction chain needs a neutron-rich environment, i.e. an electron fraction per baryon lower than 0.5, a sufficiently large entropy, and short reaction times. The neutrino-driven matter-outflow, with a time of post-bounce of the order of 10 seconds and high neutron density, is a favoured mechanism for the production of elements heavier than iron.[29] As said before, due to neutrino oscillations, the neutron abundance of the wind is modified when sterile neutrinos are included.[30]

The neutrinos determine the neutron to proton ratio, thus a possible conversion between flavours could alter this rate, and consequently the conditions needed for the r-process to take place. Calculations performed in the context of semianalytical models have shown that it is difficult to achieve the generation of the required number of free neutrons.[31] The inclusion of massive neutrinos in the formalism which describes supernovae explosions affects the cross sections involved in the reaction chains that produce heavy nuclei by modifying the abundances of the elements ejected into the interstellar medium and by changing the neutrino number densities.[24,32] In this paper, we study the impact of neutrino oscillations upon the electron fraction in the late neutrino-driven wind epoch.

This work is organized as follow. In Section 2 we present a brief description of the supernova environment and the determination of the electron fraction. In Section 3 we present the formalism needed to calculate the neutrino densities and show the results of the calculations in Section 4. In order to estimate the differences between our results and the results obtained by applying other approximations,[24,41,42] we have performed calculations of the electron fraction Y_e as a function of the stellar radius, by using power-law and Fermi-Dirac distributions, as discussed in section 4. The conclusions are drawn in Section 5.

2. Stellar environment

The neutrino driven-wind is generated after the rebound of the collapsing star. For large radius, that is outside the region where the reheating mechanism takes place, the hydrostatic equilibrium is reached leading to[23]

$$\frac{dP}{dr} = \frac{-G\rho M_{NS}}{r^2}\,, \tag{1}$$

where P is the hydrostatic pressure, G is the gravitational constant, M_{NS} is the mass of the proto-neutron star and ρ is the matter density. Since the entropy at constant chemical potential is related to the pressure as $S = \frac{\partial P}{\partial T}$ one can integrate Eq. (1) to obtain

$$TS = \frac{G m_b M_{NS}}{r}\,. \tag{2}$$

In the last expression m_b is the baryon mass. Near the star the radiation is the main contribution and the entropy can be written as

$$\frac{S}{k_B} = \frac{2\pi^2 g_s}{45\rho_b}\left(\frac{k_B T}{\hbar c}\right)^3\,, \tag{3}$$

where k_B is the Boltzmann constant, ρ_b is the baryon density and $g_s = \sum_{boson} g_b + \frac{7}{8}\sum_{fermion} g_f$ is the number of degrees of freedom.[23]

Direct comparison between the last two equations yields

$$\rho_b \simeq 38\frac{2}{11} g_s \frac{M_{NS}^3}{S_{100}^4 r_7^3}\,, \tag{4}$$

in units of $10^3 \mathrm{gr\,cm^{-3}}$. S_{100} represents the entropy per baryon in units of $100\,k_B$ and r_7 is the distance to the center of the star in units of 10^7 cm. The relationship between the entropy, radius and the temperature T_9 (in units of 10^9 K) is[23]

$$T_9 S_{100} \sim \frac{2.25}{r_7}\,. \tag{5}$$

Different values of the entropy indicate different stages of the supernova evolution. Small values of the entropy signal a pre-heating epoch while values larger than $100\,k_B$ describe latter stages of the evolution, such as the neutrino driven-wind.[33] We have performed the calculations with a fixed value $S_{100} = 1.5$, a value which represents the late cooling phase of the neutrino-driven wind.

To characterize the neutrinos we use a Fermi-Dirac (FD)[a] distribution function.[23] In the literature it is usual to assume a thermalized neutrino-flux, however the flux produced in a supernova does not necessarily has such a behaviour. The departure from thermalization is accounted for by a renormalization of the distribution function with a factor ξ_s. The renormalized FD distribution function will be denoted $f_\nu(E_\nu)$ in the following equations.

[a]In Section IV we have also considered a power-law distribution as suggested in Ref.[24, 41]

The flux can be obtained, after integration on solid-angles as[23]

$$\frac{d\phi_\nu}{dE_\nu} = \frac{c}{8\pi^2(\hbar c)^3}\frac{R_\nu^2}{r^2}E_\nu^2 f_\nu(E_\nu)\,, \tag{6}$$

where R_ν is the radius of the neutrino-sphere. The luminosity can be computed as

$$L_\nu = \frac{cR_\nu^2}{2\pi(\hbar c)^3}\int_0^\infty E_\nu^3 f_\nu(E_\nu)dE_\nu\,. \tag{7}$$

As shown in Ref.[23,29] luminosities for different neutrino (antineutrino) species are of the order of 10^{51} erg/seg, therefore we shall adopt this estimate in our calculations.

Weak reactions modify the amount of neutrons, protons and electrons in the star through neutrino and anti-neutrino induced reactions

$$\nu_e + n \to p + e^-\,, \tag{8}$$

$$\bar{\nu}_e + p \to n + e^+\,. \tag{9}$$

The rate of these two reactions can be computed as[23]

$$\lambda_\nu = \int \sigma_\nu(E_\nu)\frac{d\phi_\nu}{dE_\nu}dE_\nu\,, \tag{10}$$

where the cross sections, in units of cm^2, are

$$\sigma_{\nu_e}(E_{\nu_e}) = 9.6\times10^{-44}\left(\frac{E_{\nu_e}+\Delta m_{np}}{MeV}\right), \tag{11}$$

$$\sigma_{\bar{\nu}_e}(E_{\bar{\nu}_e}) = 9.6\times10^{-44}\left(\frac{E_{\bar{\nu}_e}-\Delta m_{np}}{MeV}\right). \tag{12}$$

In the last expressions $\Delta m_{np} = 1.293\,\mathrm{MeV}$ is the neutron-to-proton mass-difference. Notice that for the antineutrino-cross section $\sigma_{\bar{\nu}_e}$, the antineutrino energy must be larger than the neutron-to-proton mass-difference ($E_{\bar{\nu}_e} > \Delta m_{np}$).

The reaction rates for the inverse reactions of Eqs. (8) and (9) are written:[24]

$$\lambda_{e^-} \simeq 1.578\times10^{-2}\left(\frac{T_e}{m_e}\right)^5 e^{(-1.293+\mu_e)/T_e}\left(1+\frac{0.646\mathrm{MeV}}{T_e}+\frac{0.128\mathrm{MeV}^2}{T_e^2}\right), \tag{13}$$

$$\lambda_{e^+} \simeq 1.578\times10^{-2}\left(\frac{T_e}{m_e}\right)^5 e^{(-0.511-\mu_e)/T_e} \times\left(1+\frac{0.1.16\mathrm{MeV}}{T_e}+\frac{0.601\mathrm{MeV}^2}{T_e^2}+\frac{0.178\mathrm{MeV}^3}{T_e^3}+\frac{0.035\mathrm{MeV}^4}{T_e^4}\right). \tag{14}$$

In these expression m_e, μ_e and T_e are the electron mass, the electron chemical potential and the electron temperatures (in units of MeV) and the rates are given in units of s^{-1}. The electron chemical potential, at a fixed temperature, can be obtained from the equation

$$Y_e = \frac{8\pi}{3N_b}T_e^2\mu_e\left(\left(\frac{\mu_e}{T_e}\right)^2+\pi^2\right), \tag{15}$$

where Y_e is the electron fraction.

Calling N_j and A_j the density and mass-number of particles of the nuclear j-specie, respectively, the fraction of that given specie is

$$Y_j = \frac{X_j}{A_j} = \frac{N_j}{\sum_i N_i A_i}\,. \tag{16}$$

If the environment is electrically neutral, the electron fraction can be computed as[24]

$$Y_e = \sum_j Z_j Y_j = X_p + \frac{1}{2}X_\alpha + \sum_k \frac{Z_k}{A_k} X_k\,, \tag{17}$$

where Z_j is the charge of the j-specie. The quantities X_p, X_α and X_k are the fraction mass of proton, helium and heavy nuclei, respectively.

Considering the weak reactions of Eqs. (8)-(9)), the proton fraction mass varies as

$$\frac{dX_p}{dt} = -(\lambda_{\bar{\nu}_e} + \lambda_{e^-})X_p + (\lambda_{\nu_e} + \lambda_{e^+})X_n\,. \tag{18}$$

In the absence of heavy-elements the time dependence of the electron-fraction is equal to the one of protons. Also, in this case, the sum of the fraction masses of neutrons, protons and α-particles is given by the relation $X_p + X_n + X_\alpha = 1$. Taking this into account the previous equation reads

$$\frac{dY_e}{dt} = \lambda_n - (\lambda_p + \lambda_n)Y_e + \frac{1}{2}(\lambda_p - \lambda_n)X_\alpha\,, \tag{19}$$

where $\lambda_p = \lambda_{\bar{\nu}_e} + \lambda_{e^-}$ and $\lambda_n = \lambda_{\nu_e} + \lambda_{e^+}$.

If the plasma reaches a stage of weak equilibrium, the electron fraction does not change with time, that is $\frac{dY_e}{dt} = 0$ and, therefore

$$Y_e = \frac{\lambda_n}{\lambda_n + \lambda_p} + \frac{1}{2}\frac{\lambda_p - \lambda_n}{\lambda_p + \lambda_n} X_\alpha\,. \tag{20}$$

In the previous equation we have considered X_α as a time independent quantity. To perform the calculations we have taken different values of this quantity, starting from $X_\alpha = 0$.

3. Neutrino densities

In this section we introduce the differential equation needed to compute the neutrino distribution-function as a function of the star radius. Calling ρ ($\bar{\rho}$) to the neutrino (antineutrino)-distribution function in its matrix form and $\mathcal{H}$ ($\bar{\mathcal{H}}$) the neutrino (antineutrino) Hamiltonian in the flavor basis, the differential equations that give the dependence of the neutrino (antineutrino) distribution functions upon the radius are[23,24]

$$\begin{aligned} i\frac{\partial \rho}{\partial r} &= [\mathcal{H}, \rho]\,, \\ i\frac{\partial \bar{\rho}}{\partial r} &= \left[\bar{\mathcal{H}}, \bar{\rho}\right]\,. \end{aligned} \tag{21}$$

The Hamiltonian can be written as

$$\mathcal{H} = \mathcal{H}^{vac} + \mathcal{H}^{m} + \mathcal{H}^{\nu-\nu}\,, \tag{22}$$

where $\mathcal{H}^{vac}$ describes neutrino oscillations in vacuum, $\mathcal{H}^{m}$ represents the neutrino-matter interactions and $\mathcal{H}^{\nu-\nu}$ takes into account the neutrino-neutrino interactions. In this treatment of $\nu-\nu$ interactions we assume the single-angle approximation in which all neutrinos feel the same neutrino-neutrino refractive effect.[34,35] Some works suggest that for non-shallow matter density profiles averaging over neutrino trajectories plays a minor role in the final outcome.[36]

3.1. *Active-sterile neutrino mixing,* $1+1$*-scheme*

The active-sterile neutrino mixing in the $1+1$-scheme is described by the Hamiltonian

$$\mathcal{H}^{vac}_{mass} = pc \begin{pmatrix} 1+\frac{m_1^2c^2}{2p^2} & 0 \\ 0 & 1+\frac{m_4^2c^2}{2p^2} \end{pmatrix}. \tag{23}$$

where we have taken $E_i = \sqrt{p^2c^2+m_i^2c^4} \approx pc + \frac{m_i^2c^3}{2p}$, m_i stands for the mass of the eigenstate i, and p is the momentum. The mixing matrix can be written as

$$U = \begin{pmatrix} c_{14} & s_{14} \\ -s_{14} & c_{14} \end{pmatrix}, \tag{24}$$

where we have used the notation $c_{ij} = \cos\theta_{ij}$ and $s_{ij} = \sin\theta_{ij}$. The Hamiltonian in the flavour basis reads

$$\mathcal{H}^{vac} = \left(pc + \frac{m_1^2c^3}{2p}\right)\begin{pmatrix} 1 & 0 \\ 0 & 1 \end{pmatrix} + \frac{\Delta m_{14}^2 c^3}{2p}\begin{pmatrix} s_{14}^2 & c_{14}s_{14} \\ c_{14}s_{14} & c_{14}^2 \end{pmatrix}, \tag{25}$$

where $\Delta m_{14}^2 = m_4^2 - m_1^2$.

Assuming that the sterile neutrino cannot interact with the electrons or neutrons in the star,[24] the electron neutrino interactions with electrons and neutrons are described by the matter Hamiltonian. If the star is electrically neutral, the amount of electrons and protons is the same, that is $Y_e = Y_p$, and if one can neglect the presence of heavy particles the density of neutrons can be computed as $Y_n = 1 - Y_e$. From the definition of the electron fraction, $Y_e = \frac{N_e}{N_e+N_n}$, we can express the matter-neutrino interaction Hamiltonian as

$$\mathcal{H}^{m} = \frac{\sqrt{2}}{2} G_f N_b \begin{pmatrix} 3Y_e - 1 & 0 \\ 0 & 0 \end{pmatrix}, \tag{26}$$

where N_b is the baryon density.

For the neutrino-neutrino interactions we have considered that only the ν_e and $\bar{\nu}_e$ can interact with each other[24] and the terms involving sterile neutrinos vanish,[37] that is

$$\mathcal{H}^{\nu-\nu} = \sqrt{2} G_f \left(N_{\nu_e} - N_{\bar{\nu}_e}\right)\begin{pmatrix} 2 & 0 \\ 0 & 0 \end{pmatrix}. \tag{27}$$

where G_f is the Fermi constant and N_{ν_i} ($N_{\bar{\nu}_i}$) is the density of the i-flavour neutrino (antineutrino).[24]

3.2. *Active-sterile mixing,* $2+1$*-scheme*

In this case we are considering three types of neutrinos in the mass-basis, a light neutrino (of mass m_1), a linear combination of two heavier neutrinos, the x-neutrino of mass m_3, and a sterile neutrino of mass m_4. The Hamiltonian $\mathcal{H}^{vac}_{mass}$ reads

$$\mathcal{H}^{vac}_{mass} = pc \begin{pmatrix} 1+\frac{m_1^2c^2}{2p^2} & 0 & 0 \\ 0 & 1+\frac{m_3^2c^2}{2p^2} & 0 \\ 0 & 0 & 1+\frac{m_4^2c^2}{2p^2} \end{pmatrix} . \tag{28}$$

The mixing matrix is written as

$$U = \begin{pmatrix} c_{14} & 0 & s_{14} \\ 0 & 1 & 0 \\ -s_{14} & 0 & c_{14} \end{pmatrix} \begin{pmatrix} c_{13} & s_{13} & 0 \\ -s_{13} & c_{13} & 0 \\ 0 & 0 & 1 \end{pmatrix} = \begin{pmatrix} c_{13}c_{14} & s_{13}c_{14} & s_{14} \\ -s_{13} & c_{13} & 0 \\ -c_{13}s_{14} & -s_{13}s_{14} & c_{14} \end{pmatrix} . \tag{29}$$

The Hamiltonian in the flavour basis reads

$$\mathcal{H}^{vac} = \left(pc + \frac{m_1^2c^3}{2p}\right) \begin{pmatrix} 1 & 0 & 0 \\ 0 & 1 & 0 \\ 0 & 0 & 1 \end{pmatrix} + \frac{\Delta m_{13}^2 c^3}{2p} \begin{pmatrix} c_{14}^2 s_{13}^2 & c_{14}c_{13}s_{13} & -c_{14}s_{14}s_{13}^2 \\ c_{14}c_{13}s_{13} & c_{13}^2 & -c_{13}s_{13}s_{14} \\ -c_{14}s_{14}s_{13}^2 & -s_{14}c_{13}s_{13} & s_{14}^2 s_{13}^2 \end{pmatrix}$$
$$+ \frac{\Delta m_{14}^2 c^3}{2p} \begin{pmatrix} s_{14}^2 & 0 & c_{14}s_{14} \\ 0 & 0 & 0 \\ c_{14}s_{14} & 0 & c_{14}^2 \end{pmatrix} . \tag{30}$$

The neutrino-matter interactions $\mathcal{H}^m$ can be included as described in the previous sections

$$\mathcal{H}^m = \frac{\sqrt{2}}{2} G_f N_b \begin{pmatrix} 3Y_e - 1 & 0 & 0 \\ 0 & Y_e - 1 & 0 \\ 0 & 0 & 0 \end{pmatrix} . \tag{31}$$

The neutrino-neutrino interaction-term of the Hamiltonian is written

$$\mathcal{H}^{\nu-\nu} = \sqrt{2} G_f \left(N_{\nu_e} - N_{\bar{\nu}_e}\right) \begin{pmatrix} 2 & 0 & 0 \\ 0 & 1 & 0 \\ 0 & 0 & 0 \end{pmatrix} + \sqrt{2} G_f \left(N_{\nu_x} - N_{\bar{\nu_x}}\right) \begin{pmatrix} 1 & 0 & 0 \\ 0 & 2 & 0 \\ 0 & 0 & 0 \end{pmatrix} . \tag{32}$$

4. Results

We have solved the differential equations to calculate the neutrino (antineutrino)-distribution function Eq. (21) in order to obtain the electron fraction as a function of the radius of the neutrino sphere. We have performed the calculations on the late cooling phase of the neutrino-driven wind $t_{pb} \sim 10\,\mathrm{sec}$. To solve the coupled differential equations we have adopted values for the neutrino mixing parameters

given in the literature.[38,39] As initial condition we have taken at the neutrino sphere radius $R_\nu = 10\,\text{Km}$ a Fermi-Dirac neutrino distribution-function. The mean-energies were extracted from Refs.,[23,29] namely: $< E_{\nu_e} >= 10\,\text{MeV}$, $< E_{\overline{\nu}_e} >= 15\,\text{MeV}$, $< E_{\nu_x} >=< E_{\overline{\nu}_x} >= 24\,\text{MeV}$. For the sterile neutrino, we have multiplied the distribution function by a factor, ξ_s, which is taken as a free parameter. All the calculations have been performed assuming different values for the mass fraction of α particles, $X_\alpha = 0,\ 0.3$ and 0.5. We have repeated some of the calculations using a power-law distribution[24,41] to compute Y_e.

Active neutrinos propagate away from the SN core and convert to sterile states through MSW resonances, located at two different spacial regions. For large post bounce times inner and outer resonances are both near the neutrino-sphere. Besides neutrino interaction with matter, neutrino-neutrino interactions also affect neutrino number densities and therefore Y_e. The role of neutrino self-interactions becomes more important as post bounce increases, since the matter background is lower. For later times, $\nu_e \to \nu_s$ and $\bar{\nu_e} \to \bar{\nu_s}$ resonant conversion are expected to have the same degree of adiabaticity, resulting on a small feedback on Y_e.[41]

4.1. *Active-neutrino sterile-neutrino oscillations ($1+1$-scheme)*

Here we present the results obtained with the inclusion of a sterile neutrino in a core-collapse supernova and the effects of its interactions with active neutrinos upon Y_e. In Fig. 1 we show the results for the fraction Y_e as a function of the radius for different interactions considered in the calculations and different values of X_α. The figure shows results obtained by using a FD distribution function. For comparison we have also shown a particular case calculated with a power-law distribution function and with $X_\alpha = 0.3$ as initial condition. It can be seen that the use of a power-law distribution produces a peak at small radius and a plateau in Y_e for radius larger than 20 Km.

The calculations were performed by varying the parameter ξ_s in the interval $0 \leq \xi_s \leq 1$, the square mass difference Δm^2_{14} and the mixing angle between active and sterile-neutrinos, denoted as θ_{14}. In Fig. 2 we present the results of the electron fraction as a function of the parameter ξ_s, for two different mixing angles, $\sin^2 2\theta_{14} = 0.5$ and $\sin^2 2\theta_{14} = 0.1$, square-mass-difference $\Delta m^2_{14} = 2\,\text{eV}^2$, and for two radii. When the value of ξ_s is close to unity the electron fraction reaches a value larger than 0.5. This indicates that, in order to enhance the r-process, in the neutrino-sphere should not be sterile-neutrinos. The results are in line with the findings of Ref.[43] where the authors stated that, for the considered mass range of Δm^2_{14}, conversions to sterile neutrinos in the inner core can be neglected.

To determine the allowed values of the mixing parameters we have set an upper limit for the value of the electronic fraction, $Y_e = 0.48$, and varied the parameters with this constraint. In Fig. 3 we show the constrains on the mixing angle and the neutrino's square-mass-difference for $\xi_s = 0$, and three different radii, keeping $X_\alpha = 0$. The curves represent $Y_e = 0.48$, and the allowed regions correspond to

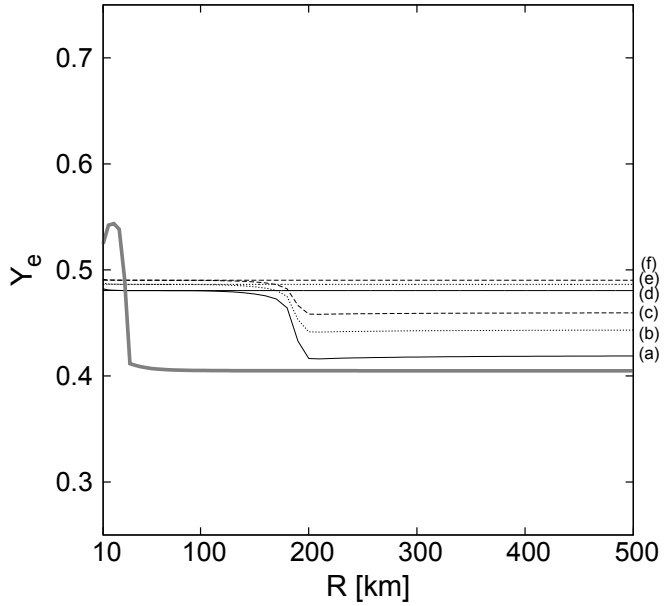

Fig. 1. Y_e as a function of the radius for the $1+1$-scheme at the late cooling time. The plot was made for $\Delta m^2_{14} = 2\,\mathrm{eV}^2$ and $\sin^2 2\theta_{14} = 0.16$. The curves labelled (a), (b) and (c) stand for $X_\alpha = 0$, $X_\alpha = 0.3$ and $X_\alpha = 0.5$ when all the interactions are considered in the Hamiltonian. The curves labelled (d), (e) and (f) stand for $X_\alpha = 0$, $X_\alpha = 0.3$ and $X_\alpha = 0.5$ when only oscillations in vacuum are considered in the Hamiltonian. The calculations were made using a Fermi-Dirac distribution to describe the initial condition of neutrinos. The thicker line shows the results obtained by using a power-law distribution[24,41] and for $X_\alpha = 0.3$.

$\Delta m^2_{14} > 1.5\,\mathrm{eV}^2$ for R = 150 Km, $\Delta m^2_{14} > 1\,\mathrm{eV}^2$ for R = 200 Km and $\Delta m^2_{14} > 0.5\,\mathrm{eV}^2$ for R = 250 Km. The comparison between our results and those of Ref.,[43] for the case of the $1+1$ scheme and later epoch, shows that the set of parameters where the r-process is favoured are common to both results. The region is determined by the limits $0.5\,\mathrm{eV}^2 < \Delta m^2_{14} < 10^2\,\mathrm{eV}^2$. For larger values of X_α we have found that $Y_e > 0.5$, therefore suppressing the formation of heavy nuclei via r-process.

In Fig. 4 we show the allowed values of Δm^2_{14} and ξ_s (white regions) for different values of X_α, using all the interactions in the calculation of the electronic fraction, for a neutron-rich environment. The values that yield $Y_e < 0.48$ are consistent with small values of ξ_s. If the mixing angle increases its value the factor ξ_s must decrease in order to ensure the effectiveness of the r-process.

The allowed values for the mixing angle and the normalization constant of the sterile neutrino distribution function are presented in Fig. 5 (white regions), for two different values of the square-mass-difference. Once again, the curves correspond to the value $Y_e = 0.48$ when all the neutrino interactions are included in the calculation. The region which yields $Y_e < 0.48$ favours small values of ξ_s while the mixing-angle between active- and sterile-neutrinos is limited by the condition

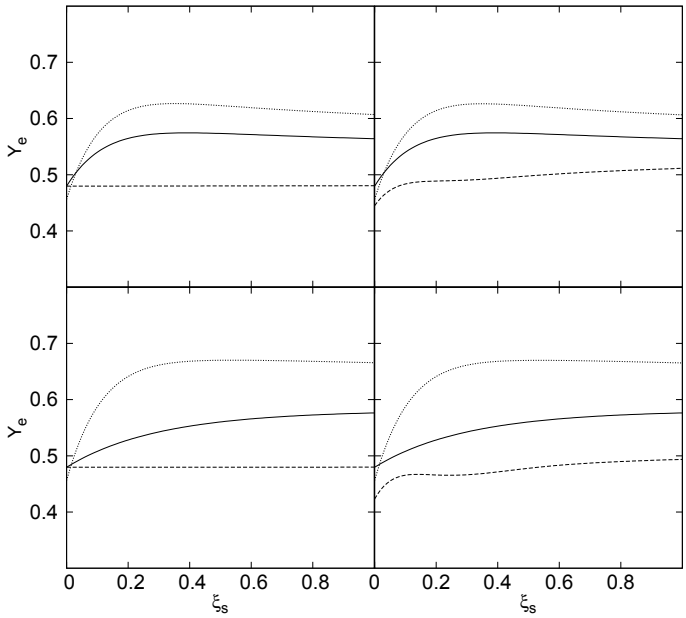

Fig. 2. Y_e as a function of the initial condition ξ_s for two different set of mixing parameters at $R = 75\,\mathrm{Km}$ (first column) and $R = 250\,\mathrm{Km}$ (second column) in the $1+1$-scheme. Solid line: only active-sterile neutrino oscillations; dotted line: oscillations and neutrino-matter interactions; dashed-line: oscillations, neutrino-matter and neutrino-neutrino interactions. Top row: $\sin^2 2\theta_{14} = 0.5$; bottom row: $\sin^2 2\theta_{14} = 0.1$. In all figures we assume normal hierarchy for the sterile squared-mass-difference $\Delta m^2_{14} = 2\,\mathrm{eV}^2$, implying that the neutrino mass eigenstate ν_4 is heavier than the mass eigenstates of the active neutrinos.

$\sin^2 2\theta_{14} < 0.6$ when $\Delta m^2_{14} > 2\,\mathrm{eV}^2$.

4.2. *Active-neutrino sterile-neutrino oscillations ($2+1$-scheme)*

In this section we show the effects of the inclusion of sterile neutrinos in a SN-type environment when the sterile neutrino can mix with one of the two active neutrinos, namely the electron-neutrino. The mixing-angle between active-neutrinos considered in this calculation is $\sin^2 2\theta_{13} = 0.09$ and the square-mass-difference $\Delta m^2_{13} = 2 \times 10^{-3}\,\mathrm{eV}^2$. We assume a normal-mass-hierarchy for the atmospheric neutrinos.[38] In Fig. 6 we show the behaviour of the electron fraction as a function of the radius for the different interactions. This computation were performed mostly for a FD distribution function as initial condition of Eq. (21) (thin lines) and using a power-law distribution function[24,41,42] for $X_\alpha = 0.3$ (thick line).

In Fig. 7 we present the results of the electron-fraction Y_e as a function of the constant ξ_s, at $R = 75\,\mathrm{Km}$ and R $= 250\,\mathrm{Km}$. It is observed that the value of the electron-fraction is larger than 0.5 if the neutrino-neutrino interactions are not included in the calculation.

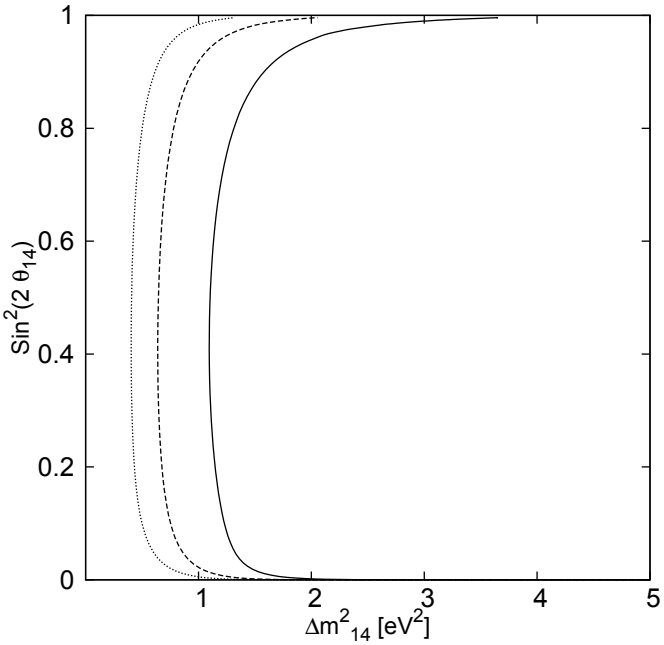

Fig. 3. Active-sterile mixing parameters for different radii in the $1+1$-scheme and for $X_\alpha = 0$. The lines stand for $Y_e = 0.48$ as a limiting value, calculated using all the interactions in the neutrino sector and for different radii: solid line: R = 150 Km; dashed line: R = 200 Km; dotted line: R = 250 Km. The values of the parameters for which the r-process is favoured are determined by the region at the right-side of each curve, since for these regions $Y_e < 0.48$.

In Fig. 8 we show the values of the mixing-angle and the square-mass-difference, between active and sterile-neutrinos, for $\xi_s = 0$ and $Y_e = 0.48$. The condition $\Delta m^2_{14} > 2\,\mathrm{eV}^2$ is consistent with the r-process at small radius. This value decreases if the radius increases. In the calculations we set $X_\alpha = 0$ since for larger values of X_α we found $Y_e > 0.5$.

In Fig. 9 we show the allowed values of Δm^2_{14} and ξ_s (white regions) for different values of the active-sterile mixing angle and several values of X_α. If $\Delta m^2_{14} > 1.8\,\mathrm{eV}^2$ and $\xi_s < 0.45$ the electron fraction becomes lower than 0.48 for small mixing angles. For larger mixing-angles the constraint $Y_e < 0.48$ gives smaller values for the constant ξ_s and does not affect the constraint on the square-mass-difference.

The constraints on the mixing-angle and the normalization constant of the sterile neutrino distribution functions are more stringent than in the $1+1$-scheme as we can see in Fig. 10. In this case, for $\Delta m^2_{14} = 2\,\mathrm{eV}^2$, the mixing angle should be lower than 0.55 ($\sin^2 2\theta_{14} < 0.8$) and $\xi_s < 0.1$, in order to obtain $Y_e < 0.5$.

As general features of our results we can mention that the inclusion of the sterile neutrino have an important effect upon Y_e, since the value of the electron fraction can be drastically reduced when all the channels (oscillations, matter interactions and neutrino interactions) are considered. The allowed region of the space of pa-

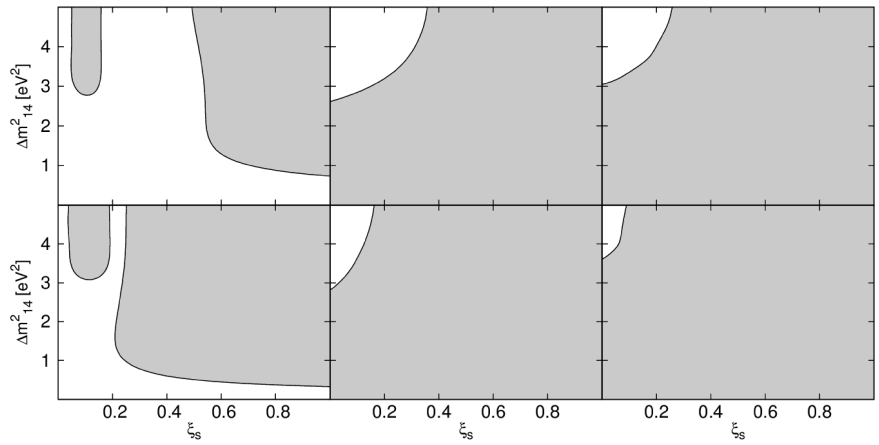

Fig. 4. Values of Δm^2_{14} and ξ_s for two different values of the mixing angle θ_{14} and $R = 150\,\mathrm{Km}$ in the $1+1$-scheme. First row corresponds to $\sin^2 2\theta_{14} = 0.1$ and second row for $\sin^2 2\theta_{14} = 0.5$. First, second and third columns stand for $X_\alpha = 0$, 0.3 y 0.5 respectively. White regions represent the combinations of parameters which favour the r-process ($Y_e < 0.48$), gray regions correspond to the combinations of parameters that generate $Y_e > 0.48$.

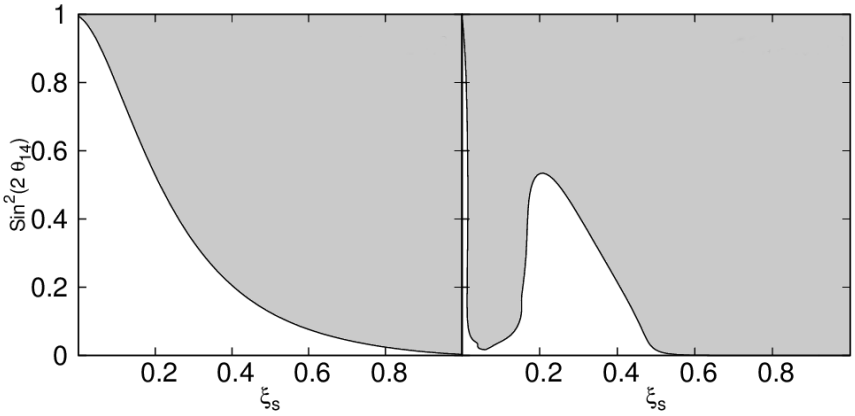

Fig. 5. Values of $\sin^2 2\theta_{14}$ and ξ_s for two different values of the square-mass-difference Δm^2_{14} and $\mathrm{R} = 150\,\mathrm{Km}$ ($1+1$-scheme). Left figure: $\Delta m^2_{14} = 2\,\mathrm{eV}^2$; right figure: $\Delta m^2_{14} = 10\,\mathrm{eV}^2$. White regions represent the combinations of parameters that favours the occurrence of the r-process, while gray regions correspond to the combinations of parameters that generate $Y_e > 0.5$. The plot was made for $X_\alpha = 0$. Larger values of X_α yields $Y_e > 0.5$

rameters favours a small value of the renormalization factor (hindrance factor) ξ_s. Also, the allowed regions of parameters are strongly reduced when the value of X_α is increased.

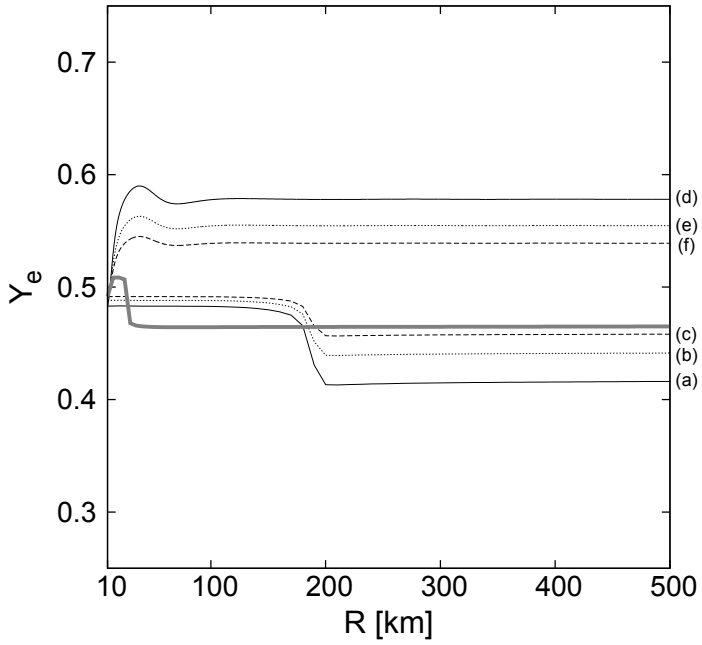

Fig. 6. Y_e as a function of the radius in the $2+1$-scheme for the late cooling time. The plot was made for $\Delta m^2_{13} = 2\times10^{-3}\,\mathrm{eV}^2$, $\Delta m^2_{14} = 2\,\mathrm{eV}^2$, $\sin^2 2\theta_{13} = 0.09$ and $\sin^2 2\theta_{14} = 0.16$. The curves labelled (a), (b) and (c) stand for $X_\alpha = 0$, $X_\alpha = 0.3$ and $X_\alpha = 0.5$ when all the interactions are considered in the Hamiltonian. The curves labelled (d), (e) and (f) stand for $X_\alpha = 0$, $X_\alpha = 0.3$ and $X_\alpha = 0.5$ when only oscillations in vacuum are considered in the Hamiltonian. The calculations were performed using a Fermi-Dirac distribution to describe the initial condition of neutrinos. The thicker line displays the results obtained for $X_\alpha = 0.3$ and by using the distribution function of.[24, 41]

5. Conclusions

In this work we have studied the impact of the inclusion of massive sterile neutrinos upon the physical conditions required for the occurrence of the r-process in supernovae. The analysis was performed by calculating the electron-fraction in the stellar interior as a function of the sterile-active neutrino mixing parameters. We have found that the electron abundance is sensitive to the inclusion of sterile neutrinos, and that it depends on the neutrino interactions, e. g. neutrino-neutrino interactions or neutrino-matter interactions. From our results, the onset of the r-process in presence of a sterile neutrino, is compatible with the limits $\Delta m^2_{14} \geq 2\mathrm{eV}^2$, $\sin^2 2\theta_{14} < 0.8$, and $\xi_s < 0.5$, for the square-mass-difference, mixing-angle and enhancement factor of the sterile neutrino sector, respectively. As explained in the text, we found that the r-process is strongly affected by the fraction X_α.

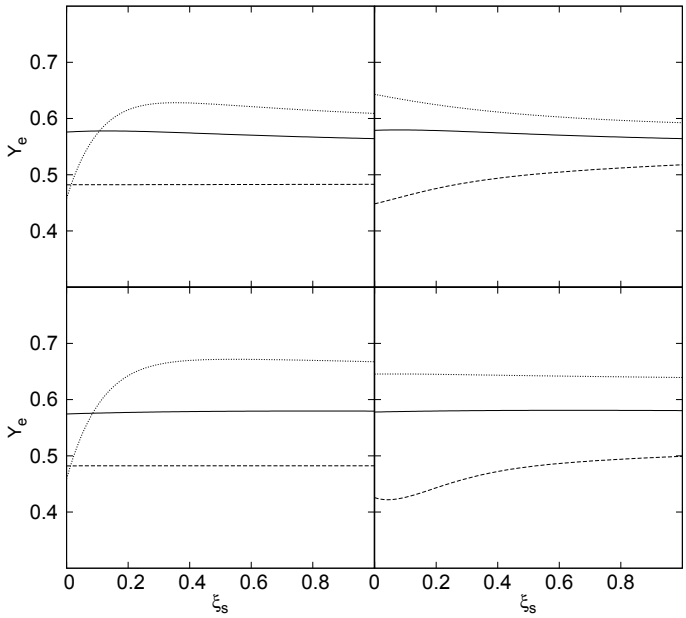

Fig. 7. Y_e as a function of the initial condition ξ_s, in the $2+1$-scheme, for two different set of mixing parameters at R = 75 Km (first column) and R = 250 Km (second column). Solid line: only oscillations; dotted line: oscillations and neutrino-matter interactions and oscillations; dashed-line: neutrino-matter and neutrino-neutrino interactions. Top figure: $\sin^2 2\theta_{14} = 0.5$; bottom figure: $\sin^2 2\theta_{14} = 0.1$, both sets of results have been obtained with $\Delta m^2_{14} = 2\,\mathrm{eV}^2$.

Acknowledgment

This work was supported by grant (PIP-616) of the National Research Council of Argentina (CONICET), and by a research-grant of the National Agency for the Promotion of Science and Technology (ANPCYT) of Argentina. O. C. and M. E. M. are members of the Scientific Research Career of the CONICET.

References

1. LSND Collaboration, A. Aguilar et al., Phys. Rev. D **64**, 112007 (2001).
2. Super-Kamiokande Collaboration, K. Abe et al., Phys. Rev. D **83**, 052010 (2011).
3. SNO Collaboration, B. Aharmim et al., Phys. Rev. C **87**, 015502 (2013).
4. MiniBooNE Collaboration, A. A. Aguilar-Arevalo et al., Phys. Rev. Lett. **110**, 161801 (2013).
5. CHOOZ Collaboration, M. Apollonio et al., Phys. Lett. B **466**, 415 (1999).
6. SAGE Collaboration, J. N. Abdurashitov et al., Phys. Rev. C **80**, 015807 (2009).
7. Kamland Collaboration, A. Gando et al., Phys. Rev. D **83**, 052002 (2011).
8. GNO Collaboration, M. Altmann et al., Phys. Lett. B **616**, 174 (2005).
9. K2K Collaboration, M. H. Ahn et al., Phys. Rev. D **74**, 072003 (2006).
10. Borexino Collaboration, C. Arpesella et al., Phys. Rev. Lett. **101**, 091302 (2008).
11. C. Athanassopoulos et al., Phys. Rev. Lett. **75**, 2650 (1995).

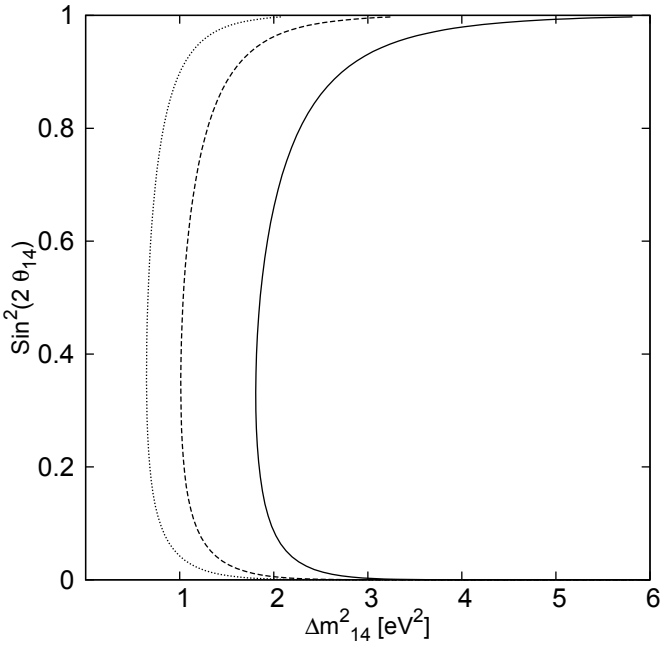

Fig. 8. Parameters consistent with the r-process in the 2+1 scheme. The results are shown in the same way of Figure 3. The lines stand for $Y_e = 0.48$, calculated using all the interactions in the neutrino sector. Solid line: $R = 150\,\mathrm{Km}$; dashed line: $R = 200\,\mathrm{Km}$; dotted line: $R = 250\,\mathrm{Km}$.

12. C. Athanassopoulos et al., Phys. Rev. Lett. **77**, 3082 (1996).
13. A. A. Aguilar-Arevalo et al., Phys. Rev. Lett. **98**, 231801 (2007).
14. A. Boyarsky, O. Ruchayskiy and M. Shaposhnikov, Ann. Rev. Nucl. Part. Sci. **59**, 191 (2009).
15. R. N. Mohapatra and P. B. Pal, Massive Neutrinos in Physics and Astrophysics (2004), World Scientific.
16. G. G. Raffelt, Nucl. Phys. Proc. Suppl. **95**, 183 (2001).
17. O. Civitarese, M. E. Mosquera, and M. M. Sáez, IJMPE **23**, 1450080 (2014).
18. Y. Z. Qian et al., Phys. Rev. Lett. **71**, 1965 (1993).
19. Y. Z. Qian and G. M. Fuller, Phys. Rev. D **51**, 1479 (1995).
20. A. Molinari, L. Riccati and W. M. Alberico, From Nuclei and Their Constituents to Stars (2003), IOS Press.
21. K. G. Balasi, K. Langanke, and G. Martinez-Pinedo, Prog. Part. Nucl. Phys. **85**, 33 (2015).
22. J. Fetter et al., Astropart. Phys. **18**, 433 (2003).
23. A. Balantekin and H. Yuksel, New J. Phys. **7**, 51 (2005).
24. I. Tamborra et al., JCAP **1**, 13 (2012).
25. M.-R. Wu, G. Martinez-Pinedo, and Y.-Z. Qian, in 13th International Symposium on Origin of Matter and Evolution of the Galaxies (OMEG2015) Beijing, China, June 24-27 (2015).
26. H.-T. Janka, Ann. Rev. Nucl. Part. Sci. **62**, 407 (2012).
27. S. Pastor, G. G. Raffelt, and D. V. Semikoz, Phys. Rev. D **65**, 053011 (2002).
28. S. E. Woosley et al., Astrophys. J. **433**, 229 (1994).

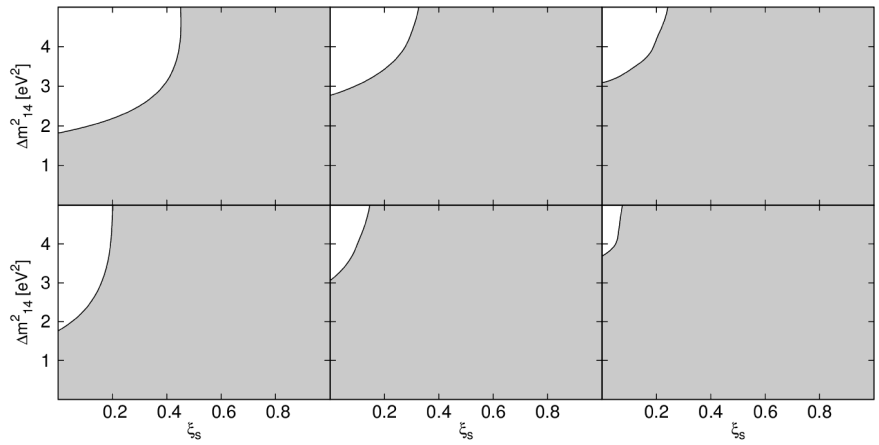

Fig. 9. Allowed values of Δm^2_{14} and ξ_s for two different values of the mixing angle θ_{14} and for $R = 150\,\mathrm{Km}$ $(2+1$-scheme). First row corresponds to $\sin^2 2\theta_{14} = 0.1$ and second row for $\sin^2 2\theta_{14} = 0.5$. First, second and third column stands for $X_\alpha = 0$, 0.3 y 0.5 respectively. The curves show the results which obey the constraint $Y_e = 0.48$. White regions represent the combinations of parameters favourable for the production r-process, while gray regions correspond to the combinations of parameters that generate $Y_e > 0.48$.

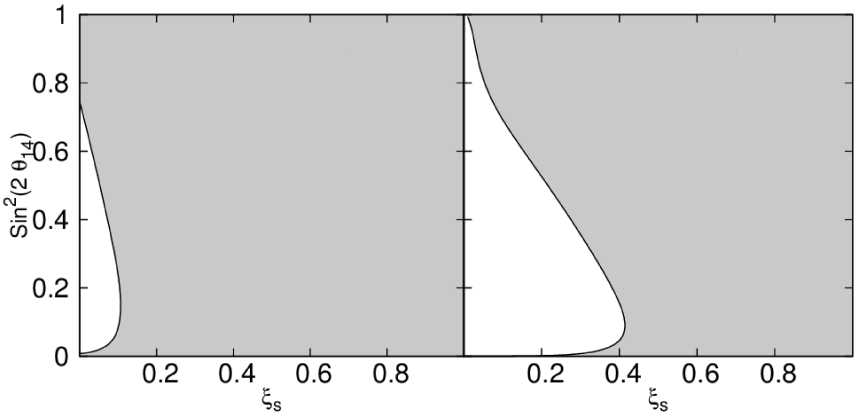

Fig. 10. Allowed values of $\sin^2 2\theta_{14}$ and ξ_s for two values of the of square-mass-difference Δm^2_{14} and for $R = 150\,\mathrm{Km}$ $(2+1$-scheme). Left figure: $\Delta m^2_{14} = 2\,\mathrm{eV}^2$; right figure: $\Delta m^2_{14} = 10\,\mathrm{eV}^2$. White regions represent the combinations of parameters that favors the occurrence of the r-process, while shadowed regions correspond to cases that generate $Y_e > 0.5$. For this case we take $X_\alpha = 0$ because for larger values of X_α we have found that $Y_e > 0.5$.

29. Y.-Z. Qian, Prog. Part. Nucl. Phys. **50**, 153 (2003).
30. Y.-Z. Qian and S. E. Woosley, Astrophys. J. **471**, 331 (1996).
31. R. D. Hoffman, S. E. Woosley, and Y. Z. Qian, Astrophys. J. **482**, 951 (1997).

32. G. C. McLaughlin et al., Phys. Rev. C **59**, 2873 (1999).
33. H.-T. Janka et al., Phys. Rep. **442**, 38 (2007).
34. H. Duan , G. M. Fuller, J. Carlson, and Y.-Z Qian. Phys. Rev. D **74**, 105014 (2006).
35. H. Duan , G. M. Fuller, and Y.-Z Qian. Ann. Rev. Nucl. Part. Sci. **60**, 569-594 (2010).
36. G. L. Fogli, E. Lisi, A. Marrone and A. Mirizzi, JCAP **0712**, 010 (2007).
37. G. Sigl and G. Raffelt, Nucl. Phys. B 406 (1993) 423.
38. Double CHOOZ Collaboration, Meregaglia, A., Nuovo Cimento Geophysics Space Physics C, 38, 123 (2016).
39. H. Minakata et al., Phys. Rev. D **71**, 013005 (2005).
40. B. Dasgupta, G. G. Raffelt and I. Tamborra, Phys. Rev. D **81**, 073004 (2010).
41. E. Pllumbi, I. Tamborra, S. Wanajo, H. T. Janka and L. Hüdepohl. Astrophys. J. **808**, 188 (2015).
42. M. T. Keil, G. G. Raffelt, and H.-T. Janka, Astrophys. J. **590**, 971 (2003).
43. H. Nunokawa, J. T. Peltoniemi, A. Rossi and J. W. F. Valle, Phys. Rev. D **56**, 1704 (1997).
44. L. Hüdepohl, B. Müller, H.-T. Janka, A. Marek, and G. G. Raffelt, Phys. Rev. Lett **104**, 251101 (2010).